

Improved Υ Spectrum with Dynamical Wilson Fermions.

N. Eicker, Th. Lippert, K. Schilling, A. Spitz*

HLRZ, Forschungszentrum Jülich, 52425 Jülich and

DESY, 22603 Hamburg, Germany

J. Fingberg, S. Güsken, H. Hoerber[†], J. Viehoff

Fachbereich Physik, Bergische Universität, Gesamthochschule Wuppertal

Gaußstraße 20, 42097 Wuppertal, Germany

SESAM collaboration

(August 1, 2018)

Abstract

We present results for the $b\bar{b}$ spectrum obtained using an $\mathcal{O}(M_b v^6)$ -correct non-relativistic lattice QCD action, where M_b denotes the bare b-quark mass and v^2 is the mean squared quark velocity. Propagators are evaluated on SESAM's three sets of dynamical gauge configurations generated with two flavours of Wilson fermions at $\beta = 5.6$. These results, the first of their kind obtained with dynamical Wilson fermions, are compared to a quenched analysis at equivalent lattice spacing, $\beta = 6.0$. Using our three sea-quark values we perform the “chiral” extrapolation to $m_{\text{eff}} = m_s/3$, where m_s denotes the strange quark mass. The light quark mass dependence is found to be small in relation to the statistical errors. Comparing the full QCD result to our quenched simulation we find better agreement of our dynamical data with experimental results in the spin-independent sector but observe no unquenching effects in hyperfine-splittings. To pin down the systematic errors we have also compared quenched results in different “tadpole” schemes as well as using a lower order action. We find

*email: spitz@hlrz.kfa-juelich.de

[†]email: hoeber@theorie.physik.uni-wuppertal.de

that spin-splittings with an $\mathcal{O}(M_b v^4)$ action are $\mathcal{O}(10\%)$ higher compared to $\mathcal{O}(M_b v^6)$ results. Relative to the results obtained with the plaquette method the Landau gauge mean link tadpole scheme raises the spin splittings by about the same margin so that our two improvements are opposite in effect.

I. INTRODUCTION

Not just since the formulation of Heavy Quark Effective Theory a few years ago [1], systems containing one or two heavy quarks have been the focus of much attention, both theoretically and experimentally. Today, B mesons are at the center of experimental efforts to determine quantities related directly to the CKM matrix, always in the hope that new physics might emerge. But, just as for systems with light quarks, the properties of hadrons containing heavy quarks are determined by non-perturbative physics and here the lattice can provide the missing link.

Non-relativistic QCD (NRQCD) [2] is an effective theory used to describe heavy quarks, $M_q \gg \Lambda_{\text{QCD}}$. The NRQCD Lagrangian is written as a series of operators expanded in powers of the mean squared heavy quark velocity v^2 , $\mathcal{L}_{\text{NRQCD}} = \sum_{i,n} c_i(g^2) O_i(M_q v^{2n})$ where the coefficients c_i are obtained by perturbative matching with QCD. The lattice version of NRQCD [3,4] allows one to simulate heavy quarks with lattice spacing errors of $\mathcal{O}(\vec{p}a)$, where p is a typical momentum $\approx \Lambda_{\text{QCD}}$, rather than the usual $\mathcal{O}(M_q a)$ for Wilson-type heavy quarks. This makes lattice NRQCD a promising technique to simulate systems containing a b -quark.

Lattice NRQCD has been widely used in the past few years to calculate a variety of phenomenologically interesting quantities (see [5] for a recent summary). The first step in the NRQCD program, naturally, is the calculation of the spectrum of the $b\bar{b}$ system. Such calculations have been performed using the quenched approximation by [6–8]. So far, there has only been one analysis of the Υ with dynamical quarks: the authors of [5,9,10] applied an $\mathcal{O}(M_b v^4)$ correct NRQCD action to gauge fields incorporating the effects of two dynamical staggered fermions¹. It was found that the experimentally known *spin-independent* spectrum could not be reproduced using the quenched approximation whereas the data with 2 dynamical fermions agrees much better. These measurements were pushed to high statistics (4% statistical errors) in [9,10] and used to obtain precision measurements of the strong coupling constant α_s . Quenching, the approximation in which the effects of dynamical fermions are disregarded, was concluded to be the largest source of uncertainty in this calculation. The dependence of the splittings on the dynamical quark *mass* was estimated, using just two mass values, to be of the same order as the statistical error. No simulation exists, so far, applying NRQCD to dynamical *Wilson* fermions.

In the *spin-dependent* sector the emerging picture is much less clear. The P-fine structure in the unquenched theory [5,10], obtained with the $\mathcal{O}(M_b v^4)$ -correct action, was found to be in very good agreement with experiment whereas the quenched results, using the same action, predict much smaller splittings. However, recent results of [8,11,12] (all of which use the quenched approximation) have exposed the sensitivity of the spin-

¹The high statistics measurements in the spin-independent sector in [9,10] were obtained using an $\mathcal{O}(M_b v^2)$ correct action.

dependent splittings to the details of the action: several improvements, such as the inclusion of higher order spin-dependent terms in the NRQCD expansion, the addition of lattice-artefacts correcting terms of $\mathcal{O}(a^2)$ [8,12] as well as an improved phenomenological estimate of the coefficients c_i [12,13] were found to have sizeable effects of $\mathcal{O}(10 - 20\%)$ for these splittings. Thus, there has recently been strong support in favour of using the $\mathcal{O}(M_b v^6)$ -correct NRQCD action, where, at highest order, all *spin-dependent* corrections are added, as well as for the use of the mean link Landau gauge tadpole scheme to estimate the perturbative coefficients c_i . The effects of these improvements for dynamical configurations have not been studied.

In the simulation presented here we attempt to address many of the open issues pinpointed above. Using SESAM's large sample of dynamical Wilson-fermion gauge configurations we study both the spin-independent as well as the spin-dependent spectrum of the Υ . Our strategy, in searching for sea-quark effects, will be to compare our final dynamical results to that of a quenched simulation at equivalent lattice spacing. Thus, we hope to consolidate that unquenching brings the spin-independent splittings into good agreement with experiment. Using our three sea-quark masses we can also study the dependence of mass-splittings on the light sea-quark mass. Following the recent suggestions of [8,12] we have implemented the NRQCD action including spin-dependent corrections of $\mathcal{O}(M_b v^6)$ and we remove tadpoles using the mean link calculated in Landau gauge. With these ingredients we hope to clarify the effect of unquenching in the spin-dependent splittings. In addition, using the quenched configurations we investigate: (i) the effect of changing tadpole prescriptions; (ii) the effect of using an $\mathcal{O}(M_b v^4)$ correct action compared to the $\mathcal{O}(M_b v^6)$ corrected one.

II. SIMULATION DETAILS

In section II A we present the discretized version of our $\mathcal{O}(M_b v^6)$ correct NRQCD action. Section II B addresses issues concerning the determination of the perturbative coefficients $c_i(g^2)$.

A. Action

The non-relativistic (Euclidean) lattice Hamiltonian to $\mathcal{O}(M_b v^6)$ consists of [3]: the kinetic energy operator,

$$H_0 = -\frac{\Delta^{(2)}}{2M_b}, \quad (1)$$

which is of order $M_b v^2$; relativistic corrections of order $M_b v^4$,

$$\delta H^{(4)} = -c_1 \frac{(\Delta^{(2)})^2}{8M_b^3} + c_2 \frac{ig}{8M_b^2} (\Delta \cdot E - E \cdot \Delta)$$

$$\begin{aligned}
& -c_3 \frac{g}{8M_b^2} \boldsymbol{\sigma} \cdot (\tilde{\Delta} \times \tilde{\mathbf{E}} - \tilde{\mathbf{E}} \times \tilde{\Delta}) - c_4 \frac{g}{2M_b} \boldsymbol{\sigma} \cdot \tilde{\mathbf{B}} \\
& + c_5 \frac{a^2 \Delta^{(4)}}{24M_b} - c_6 \frac{a (\Delta^{(2)})^2}{16nM_b^2}, \tag{2}
\end{aligned}$$

and spin-sensitive corrections of order $M_b v^6$,

$$\begin{aligned}
\delta H^{(6)} &= -c_7 \frac{g}{8M_b^3} \{\Delta^{(2)}, \boldsymbol{\sigma} \cdot \mathbf{B}\} \\
& - c_8 \frac{3g}{64M_b^4} \{\Delta^{(2)}, \boldsymbol{\sigma} \cdot (\Delta \times \mathbf{E} - \mathbf{E} \times \Delta)\} \\
& - c_9 \frac{ig^2}{8M_b^3} \boldsymbol{\sigma} \cdot \mathbf{E} \times \mathbf{E}. \tag{3}
\end{aligned}$$

We do not include spin-independent corrections of $\mathcal{O}(M_b v^6)$. The E and B fields are defined in terms of the field strength tensor

$$\begin{aligned}
F_{\mu\nu}(x) &= -\frac{1}{4} \sum_{\square} \left(\frac{U_{\mu\nu}(x) - U_{\mu\nu}^\dagger(x)}{2i} - \frac{1}{3} \text{Tr}(\text{Im} U_{\mu\nu}(x)) \right), \\
E^i &= F^{i0}, \\
B^i &= -\frac{1}{2} \epsilon_{ijk} F^{jk}, \tag{4}
\end{aligned}$$

where, $U_{\mu\nu}$ is the standard plaquette and the sum is over all anticlockwise plaquettes in the μ - ν -plane, $1 \leq \mu \leq 4$, $1 \leq \nu < \mu$.

The removal of $\mathcal{O}(a^2 M_b v^4)$ discretization errors is achieved by: (i) using an improved version of the lattice field strength tensor [3] in the leading spin-dependent interactions (c_3 and c_4):

$$\begin{aligned}
\tilde{F}_{\mu\nu} &= \frac{5}{3} F_{\mu\nu} - \frac{1}{6} \left(U_\mu(x) F_{\mu\nu}(x + \hat{\mu}) U_\mu^\dagger(x) \right. \\
& \left. + U_\mu^\dagger(x - \hat{\mu}) F_{\mu\nu}(x - \hat{\mu}) U_\mu(x - \hat{\mu}) - (\mu \leftrightarrow \nu) \right); \tag{5}
\end{aligned}$$

(ii) adding the last two terms in $\delta H^{(4)}$ to (classically) correct for finite lattice spacing errors in the spatial and temporal derivatives and (iii) by using the improved derivative operator

$$\begin{aligned}
\tilde{\Delta}_i &= \Delta_i - \frac{a^2}{6} \Delta_i^{(+)} \Delta_i \Delta_i^{(-)} \tag{6} \\
a \Delta_i^{(+)} G(x) &= U_i(x) G(x + a\hat{i}) - G(x) \\
a \Delta_i^{(-)} G(x) &= G(x) - U_i^\dagger(x - a\hat{i}) G(x - a\hat{i}) \\
a \Delta_i G(x) &= \frac{1}{2} \left(U_i(x) G(x + a\hat{i}) - U_i^\dagger(x - a\hat{i}) G(x - a\hat{i}) \right)
\end{aligned}$$

in the leading spin-dependent interactions (c_3).

For completeness we also give our definitions of $\Delta^{(2)}$ and $\Delta^{(4)}$:

$$\begin{aligned}\Delta^{(2)} &= \sum_i \Delta_i^{(2)} \\ a^2 \Delta_i^{(2)} G(x) &= U_i(x) G(x + a\hat{i}) + U_i^\dagger(x - a\hat{i}) G(x - a\hat{i}) - 2G(x) \\ \Delta^{(4)} &= \sum_i \left(\Delta_i^{(2)}\right)^2.\end{aligned}\tag{7}$$

Following [7] the quark Greens functions are calculated from the evolution equation

$$\begin{aligned}G(t+1) &= \left(1 - \frac{aH_0}{2n}\right)^n U_4^\dagger \left(1 - \frac{aH_0}{2n}\right)^n (1 - a\delta H) G(t), \\ G(0) &= \delta_{\mathbf{x},0},\end{aligned}\tag{8}$$

where $G(t)$ is a two-spinor component object.

The parameter n serves to stabilise the evolution for small bare quark masses and is set to $n = 2$ [3].

B. Tadpoles

An important feature of our simulation is the use of “tadpole”-improvement: gauge links U_μ are replaced by U_μ/u_0 where the mean link u_0 accounts for the effects of tadpole diagrams [14,15]. The coefficients c_i are then set to their tree-level values of 1.

The choice of u_0 is, of course, not unique; here we choose u_0 to be the mean value of the link variable in the Landau gauge:

$$u_0^{(L)} = \left\langle \frac{1}{3} \text{Tr} U_\mu \right\rangle, \quad \partial_\mu A_\mu = 0.\tag{9}$$

With this choice of gauge $\langle \text{Tr} U_\mu \rangle$ is maximised so that u_0 is as close to 1 as possible; it was therefore argued in [13] that remaining tadpole contributions cannot be due to lattice artefacts. A recent NRQCD lattice calculation of the $c\bar{c}$ spectrum over a variety of lattice spacings suggests that this choice improves the scaling behaviour of spectroscopic quantities [12], notably the hyperfine splittings. This view is also endorsed in [5,11] where the authors have studied the scaling behaviour in the quenched $b\bar{b}$ spectrum using three values of the coupling ($\beta = 5.7, 6.0, 6.2$), an $\mathcal{O}(M_b v^4)$ -correct action and the plaquette tadpole value (defined below). They find the spin-independent spectrum to display insignificant scaling violations whereas the hyperfine splittings do not scale that well. This is attributed partly to $\mathcal{O}(a^2)$ errors in the B field² arising in the term $\sigma \cdot B$ but partly also to the choice of plaquette tadpole improvement not capturing the tadpole

²which was obtained from the unimproved field strength tensor, eq.4.

effects sufficiently well. Additionally, two more arguments in favour of $u_0^{(L)}$ are given in [13]: firstly, the static potential shows less violation of rotational invariance using a $u_0^{(L)}$ -tadpole improved gluonic action and, secondly, the non-perturbative determination of the clover coefficient [16] is in good agreement with the $u_0^{(L)}$ -tadpole improved perturbative result. Since, for the $b\bar{b}$, all simulations performed to date, notably those with dynamical staggered quarks, have been using $u_0^{(P)} = \langle \frac{1}{3} \text{Tr} U_{\mu\nu} \rangle^{\frac{1}{4}}$, our measurement will help to explore the size of the systematic error associated with the choice of u_0 . In the quenched sector we have also performed an analysis of the S-splittings (where signals are cleanest) using the plaquette prescription and, furthermore, we compare the $\mathcal{O}(M_b v^6)$ -results to a simulation where the NRQCD action is correct to $\mathcal{O}(M_b v^4)$. In table I we compare our values of $u_0^{(L)}$ to the commonly used $u_0^{(P)}$. Note that u_0 weights the field strength tensor with four powers so that, naively, using $u_0^{(P)}$ instead of $u_0^{(L)}$ may change the hyperfine splittings by as much as 8%.

C. Correlators and Smearing

Meson correlation functions at zero momentum are built from quark propagators combined with suitable interpolating operators:

$$G_{sc,sk}^{\text{meson}}(t, \mathbf{p} = 0) = \sum_{\mathbf{x}, \mathbf{y}} \text{Tr} \left[G^\dagger(\mathbf{x}, t) \Gamma_{(sk)}^\dagger(\mathbf{y} - \mathbf{x}) \tilde{G}(\mathbf{y}, t) \right], \quad (10)$$

where the source smeared propagator \tilde{G} is obtained by evolving the extended source:

$$\tilde{G}(\mathbf{y}) = \sum_{\mathbf{x}} G(\mathbf{y} - \mathbf{x}, t) \Gamma_{(sc)}(\mathbf{x}). \quad (11)$$

The interpolating operator $\Gamma^{(sc/sk)}(\mathbf{x}) \equiv \Omega \Phi^{(sc/sk)}(\mathbf{x})$ contains a spin matrix Ω and a spatial smearing function Φ ; the superscript sc/sk denotes source and sink smearing respectively. A proper choice of Φ is crucial to obtain clear signals for excited states. Here, we benefit from a recent lattice determination of the $b\bar{b}$ potential including relativistic corrections [17]. These authors start from the $\mathcal{O}(v^4)$ non-relativistic Schrödinger-Pauli Hamiltonian [18], which, in the center of mass frame of the quark and antiquark, has the form

$$H = \sum_{i=1,2} \left(m_i + \frac{p^2}{2m_i} - \frac{p^4}{8m_i^3} + \frac{1}{8m_i^2} \nabla^2 (V_0(r) + V_a(r)) \right) + V_0(r) + V_{sd}(r, \vec{L}, \vec{S}_1, \vec{S}_2) + V_{vd}(r, \vec{p}). \quad (12)$$

It contains the central potential of Cornell type:

$$V_0(r) = V + kr - \frac{e}{r}, \quad (13)$$

spin- and velocity-dependent (sd, vd) potentials (see [17]) and the Darwin-term V_a . Following [17] we numerically integrate the radial Schrödinger equation

$$g''_{E,L}(r) = F(r, E, L, \alpha, m, k) g_{E,L}(r) \quad (14)$$

for definite radial quantum number and angular momentum, where

$$F(r, E, L, \alpha, m, k) = \frac{L(L+1)}{r^2} - m \left(E - kr + \frac{\alpha}{r} \right). \quad (15)$$

The term $-\frac{\alpha}{r}$ contains the Coulomb-term of the central potential, the $\frac{1}{r}$ contribution of the Darwin term as well as the leading $\frac{1}{r}$ contribution from V_{vd} . We leave m and k as free parameters but fix the contributions of the terms not coming from the central potential to the lattice values found in [17]. The Coulomb coefficient e is that of the quenched simulation in [17] *augmented* by 20 % to take into account the different running at short distances observed in [19]. A direct comparison with hydrogen wave functions clearly demonstrates the superiority of our choice.

The continuum wave functions are converted to the lattice using the scales obtained from SESAM's ρ -masses for each κ_{sea} . The spin matrices Ω are taken from [7] and listed in table II. Note that the finite difference operators included in table II for the P-waves are only applied in the case of delta-function smearing.

For the Υ and η_b we calculate a 4×4 matrix of correlators with four different smearings at source and sink, $sc/sk = local, 1, 2, 3$ corresponding to a point source (local), the ground state (1), the first (2) and second (3) excited states respectively. For the $L = 1$ states we restrict ourselves to the ground state and the first excitation as signals deteriorate. Correlators with momenta upto $|\mathbf{p}| = 2$ are also calculated. Gauge configurations are fixed to Coulomb gauge.

D. Lattice Parameters

The lattice parameters we have used are displayed in table III. SESAM has recently completed the generation of gauge configurations with two (degenerate) dynamical fermions at three values of the sea-quark mass. For each mass the run consists of $\mathcal{O}(5000)$ trajectories³ and we analyse every 25th trajectory giving a total of 200 configurations at each sea-quark. This is by far the largest set of dynamical Wilson-fermion gauge configurations to date, more than a factor two larger than the sample analysed with respect to NRQCD in [9]⁴. Details concerning the generation of our dynamical configurations and issues surrounding autocorrelations are discussed in ref. [20]. Here, we mention only the values of π to ρ mass ratio and the lattice spacing obtained from the ρ - which we have measured in a standard light spectrum calculation on the lattice [21,22] - for our three

³In a standard Hybrid Monte Carlo algorithm we typically set the time-step size $dt = 0.01$ and perform 100 molecular dynamics updates to generate one trajectory.

⁴The authors of [9] analyse 400 configurations taken from a total trajectory length of 2000.

dynamical sea quarks $\kappa_{\text{sea}} = \{0.156, 0.157, 0.1575\}$: $\frac{m_\pi}{m_\rho} = \{0.839(4), 0.755(7), 0.69(1)\}$ and $a_\rho^{-1} = 2.33(6)\text{GeV}$.

Taking advantage of the smallness of the bottomonium system, we exploit configurations more than once by starting the propagator evolution both at different spatial source points and on different timeslices. A binning procedure confirms that our 4 measurements per configuration are indeed independent.

Errors are obtained from correlated fits using the bootstrap procedure. They correspond to 68 % confidence limits of the distribution obtained from 300 bootstrap samples.

Throughout, we fix the bare heavy quark mass to a value $aM_b = 1.7$. In a quenched simulation by the NRQCD collaboration at $\beta = 6.0$, a bare b quark mass of 1.71 was found to yield the correct physical value of the Υ [23].

III. SPECTROSCOPY

We adopt spectroscopic notation and denote (radially excited) spin-parity eigenstates by $n^{2S+1}L_J$ (see table II).

Figure 1 shows a subset of local masses: although we have not tuned the smearing functions we generally find good plateaus for ground and excited states. For $L = 0$ the radially excited correlators remain in the first/second excitation for about ten timesteps. Local masses for P states are noisier and drop to the ground state without staying in an ‘excited plateau’ as nicely as for the S states.

A. Fitting procedures

To extract energies we fit several smearing combinations of correlators simultaneously to a multi-exponential ansatz. We find that vector fits to smeared-local propagators,

$$G_{(sc,l)}^{\text{meson}}(t) = \sum_{k=1}^{n_{exp}} b_{sc,k} e^{-E_k t} , \quad (16)$$

are quite stable whereas matrix fits appear to require higher statistics. Energy levels are obtained from correlated two-exponential fits to the two smearing functions $sc = 1, 2$ with eq. 16. Hyperfine splittings are determined from single exponential fits to the ratio

$$\frac{G_{(sc,sk)}^{\text{mesonA}}}{G_{(sc,sk)}^{\text{mesonB}}}(t) = A e^{-(E_A - E_B) \cdot t} , \quad (17)$$

thus exploiting the strong correlation between the data. We use smeared-local and smeared-smeared correlators in eq. 17. The results quoted correspond to the value with the lowest Q -fit-parameter [24] but with the statistical error enlarged to take into account the uncertainty in the fitting ranges, thus encompassing several possible fit-results from different fit-ranges. For the hyperfine splittings the errors allow for the spread in fit-results obtained using smeared-local as well as smeared-smeared data. More complicated

fit-functions confirm the results obtained from the single exponential ansatz but do not behave as stable. Results of our fits are given in tables IV and V.

B. Light quark mass dependence

We now turn to the dependence of splittings on the dynamical quark mass. Following the analysis in ref. [25] we extrapolate energy level splittings linearly in the quark mass:

$$\Delta m = \Delta m_0 + c \sum_{u,d,s} m_q, \quad (18)$$

where m_q denotes the bare light quark masses. The relevant scale we pick is given by $\frac{m_u+m_d+m_s}{3} \approx \frac{m_s}{3}$ corresponding to a “physical pion mass” of $\frac{m_\pi^2+2m_K^2}{3}$ [25,26]. Since gluon momenta inside the $b\bar{b}$ are much larger than any of the three lightest quark masses, Υ -physics should be insensitive to the $m_{u,d} - m_s$ mass-splitting. The value of the strange quark mass is taken from our recent light quark mass calculation [21] and is such that

$$m_{\text{eff}} = \frac{m_s}{3} = \frac{1}{6a} \left(\frac{1}{\kappa_s} - \frac{1}{\kappa_c} \right) \simeq 0.0156 \quad (19)$$

lies close to our lightest sea-quark mass, $am_q(\kappa = 0.1575)^5$. The authors of [25] have noted that extrapolating to $m_{\text{eff}} = \frac{m_s}{3}$ is appropriate for the 3-flavour case. In this context, we point out that there is an uncertainty in the strange quark mass m_s due to the fact that we have simulated only two (degenerate) dynamical flavours. These are identified with the up and down quarks so that, effectively, m_s is defined in the 2-flavour theory in a “partially quenched” way only [21]. Thus, it is not clear what precise value of m_{eff} mass splittings should be extrapolated to.

The extrapolations are shown for various splittings in figures 2 and 3, table VI contains $\Delta m(m_s/3)$ and Δm_0 . No significant deviation from the linear parametrization is apparent in the data. With the exception of the ${}^3S_1 - {}^1S_0$ splitting the light quark dependence is too small to be resolved given our current sensitivity. Within large errors, we find $\frac{\Delta m(m_s/3)}{\Delta m_0}$, which can be taken as an upper limit of the uncertainty in m_{eff} , to be 3 – 20% for the spin-independent splittings. Choosing $m_{\text{eff}} < m_s/3$ would have the effect of increasing the inverse lattice spacing a^{-1} (see next section). Clearly, much higher statistics is necessary to pin down these effects.

C. Lattice spacing

The lattice scale is taken from the average of the $2{}^3S_1 - 1{}^3S_1$ and $CG({}^3P) - 1{}^3S_1$ splittings at $m_s/3$ (table VII). Recall that these splittings are virtually insensitive to

⁵The three sea-quark values correspond to pions $am_\pi = \{0.445(2), 0.341(3), 0.276(5)\}$ [22].

the heavy-quark mass and vary only by a few percent from the $b\bar{b}$ to the $c\bar{c}$ ⁶. Note that the average lattice spacing for $\beta = 5.6$ for $n_f = 2$ agrees very well with the quenched one at $\beta = 6.0$ so that we can compare our results in the “full” and in the quenched theories.

The ratio of splittings, $R_{\text{SP}} = (2^3S_1 - 1^3S_1)/(CG(^3P) - 1^3S_1)$ is shown in figure 4(a) as a function of the light quark mass. All values agree with the experimental number of 1.28. Finally, we use the average lattice spacings - at $m_s/3$ in the full theory - to convert the lattice numbers to their physical values, see table VIII.

IV. DISCUSSION

Figure 5 summarizes our results for 2 and 0 flavours from table VIII. Unquenching effects are clearly visible in the spin-independent part of the $b\bar{b}$ spectrum; this is also evident from table VII which shows that the lattice spacings from the $1S - 2S$ and the $1S - 1P$ splittings do not agree in the quenched theory whereas they coincide when 2 dynamical quarks are switched on. The ratio of these splittings is plotted in figure 4(b) as a function of the number of flavours.

We do not observe any significant impact of unquenching on the hyperfine splittings. In particular, the P-hyperfine splittings seem to be underestimated for both $n_f = 0$ and $n_f = 2$. Clearly, this result needs to be corroborated with higher statistics. Errors on our hyperfine splittings encompass the statistical error as well as the uncertainty in the fitting range; the latter is essentially of the same size as the statistical error so that we can expect some improvement with higher statistics.

Compared to the only other simulation of NRQCD with dynamical quarks, performed by the NRQCD collaboration⁷ using staggered fermions [9,10], we have introduced two new features. Firstly, we have included all spin-dependent corrections to $\mathcal{O}(M_b v^6)$ and secondly, we have chosen an alternative way of removing the tadpole diagrams⁸. Compared to an $\mathcal{O}(M_b v^4)$ correct action we expect the inclusion of $\mathcal{O}(M_b v^6)$ terms to effect the hyperfine splittings on the 10 % level, since $v^2 \approx 0.1$. Performing a relatively cheap $\mathcal{O}(M_b v^4)$ quenched simulation at $\beta = 6.0$ (with 200 measurements) and calculating only the $^3S_1 - ^1S_0$ and the (spin-independent) $2S - 1S$ splittings we find this naive expectation to be very well satisfied as is shown in figure 6. Very recently, a similar effect was reported in [8] ($\mathcal{O}(10\%)$ for the $b\bar{b}$) as well as in [12], where the effect of next-to-leading

⁶The $2^3S_1 - 1^3S_1$ splittings are 562.9 and 589.1 for the $b\bar{b}$ and $c\bar{c}$ respectively; for the $CG(^3P) - 1^3S_1$ they are 439.8 ($b\bar{b}$) and 428.4 ($c\bar{c}$) - all in MeV [27].

⁷on gauge configurations generated by the HEMCGC group.

⁸Other minor differences in the two simulations are: (i) a bare b -quark mass of 1.8 was used by the NRQCD collaboration; (ii) the HEMCGC data was not “chirally” extrapolated.

order spin-dependent interactions for charmonium was found to be of $\mathcal{O}(60\%)$. Ref. [8] also found a rather severe shift, due to the $\mathcal{O}(M_b v^6)$ terms, of $\mathcal{O}(30\%)$ in the P-fine structure of the $b\bar{b}$. These results confirm Trottier’s conclusion [12] that the first three terms in the expansion for the hyperfine splitting are oscillating in sign. Therefore, the use of an $\mathcal{O}(M_b v^6)$ -correct action is mandatory to get meaningful results for the fine-structure of the Υ .

In addition to the order in the NRQCD expansion, the hyperfine splittings will be sensitive to the value of u_0 . Naively, one expects the splitting to vary as $1/u_0^4$ (since the B fields contain four links) and the ratio of the u_0^4 with the plaquette prescription to that with the mean link Landau gauge value is roughly 10 % (see table I for values of u_0 in both schemes). We therefore also plot in figure 6 the ${}^3S_1 - {}^1S_0$ splitting obtained with the $\mathcal{O}(M_b v^4)$ correct action but using the plaquette prescription for u_0 (this result is from the NRQCD collaboration⁹). The plot confirms the naive expectation and shows that changing u_0 to the mean link Landau value shifts the hyperfine splitting in the *opposite* direction as adding the $\mathcal{O}(M_b v^6)$ spin-dependent corrections. For reference the corresponding value is also shown in the spin-independent $2S - 1S$ splitting where, within the larger error, no effect is seen.

With this in mind, we compare in figure 7 our $\{\mathcal{O}(M_b v^6), u_0^{(L)}, n_f = 2\}$ results to the $\{\mathcal{O}(M_b v^4), u_0^{(P)}, n_f = 2\}$ of the NRQCD collaboration [9]. Both in the spin-independent and in the spin-dependent sectors the results are in good agreement although our splittings tend to be slightly smaller.

V. SUMMARY AND OUTLOOK

We have presented the first calculation of the $b\bar{b}$ spectrum with dynamical Wilson fermions¹⁰. Our non-relativistic lattice action is correct to $\mathcal{O}(M_b v^4)$ for spin-independent operators and includes all spin-dependent corrections of $\mathcal{O}(M_b v^6)$. We rely on tadpole improvement choosing the mean link in Landau gauge as our improvement scheme.

By use of appropriate smearing techniques we obtain clean signals for ground and excited states.

We have studied the light quark mass and flavour dependence of the $b\bar{b}$ spectrum. All quantities were linearly extrapolated to $m_s/3$. We are helped in these extrapolations by the fact that $m_s/3$ is very close to our lightest sea-quark mass so that the extrapolated values are easily consistent within errors with the values at $\kappa = 0.1575$. The lattice spacings were determined after “chiral extrapolation” with an error of 6 %, which accounts for the statistical and systematic (fitting) uncertainties.

⁹We have reproduced their value on 200 configurations but with a larger error.

¹⁰We note that the authors of [28] are presently starting a similar analysis.

Comparing to the quenched calculation at similar lattice spacing we find a distinct unquenching effect in the spin-independent splittings which can be quantified by the ratio $R_{\text{SP}} = \frac{2^3 S_1 - 1^3 S_1}{1^P - 1^3 S_1}$ determined to be 1.23(11) with 2 dynamical flavours and 1.43(9) for the quenched case; the experimental value is 1.28.

We have estimated the systematic error arising due to two different choices of the tadpole subtraction factor u_0 ; whereas spin-independent quantities remain unaffected by changes in u_0 the fine splittings increase when using the mean link Landau gauge u_0 . Interestingly, we find this effect to be of the same magnitude but of *opposite* direction as switching on the spin-dependent $\mathcal{O}(M_b v^6)$ corrections. These two effects thus combine to yield good agreement between our $\{\mathcal{O}(M_b v^6), u_0^{(L)}, n_f = 2\}$ results and the $\{\mathcal{O}(M_b v^4), u_0^{(P)}, n_f = 2\}$ results of the NRQCD collaboration with dynamical staggered fermions [9].

Our results confirm that the $\mathcal{O}(M_b v^6)$ terms in the action are mandatory for calculating the hyperfine splittings. As expected, the determination of the lattice spacing a^{-1} (as used, for example, in the determination of α_s [10]) remains unaffected by changing tadpole schemes.

Overall, NRQCD has proven to work very well in the spin-independent sector, in particular in giving a precise determination of the lattice spacing a . Given the weak dependence of these splittings on the heavy quark (experimentally) as well as on the light quark masses, as found here, it appears worthwhile to push the scale determinations to higher statistics using our configurations generated by T χ L at $\kappa = 0.1575$ on $24^3 \times 40$ lattices ($\beta = 5.6$). This would enable a reliable extrapolation to 3 or 4 flavours. The dominant source of error in such a lattice scale determination is most likely due to the remaining lattice discretisation errors in the gauge configurations.

Although higher statistics are highly desirable, it seems unlikely that progress in the spin-dependent sector will come from this approach alone. It is worrying to find the spin-dependent corrections of $\mathcal{O}(M_b v^6)$ as large as 10 % even for the $b\bar{b}$, decreasing the fine-splittings relative to the lower order estimates. Even at this order the NRQCD expansion does not describe the hyperfine structure of the spectrum. A perturbative or non-perturbative calculation of the coefficients c_i is badly needed¹¹.

ACKNOWLEDGEMENTS

H. H. and A. S. wish to thank C. Davies for a number of fruitful discussions. We thank A. Wachter for the kind donation of his Schrödinger equation solver!

We appreciate support by EU network grant No. ERB CHRX CT 92-0051. A. S. acknowledges support of the DFG-Graduiertenkolleg. Part of the computations have been

¹¹Work in this direction was recently started by [29]. Perturbative calculations [30] indicate that radiative corrections to c_1 and c_5 are small.

performed on the Connection Machine CM-5 of the Institut for Angewandte Informatik, Wuppertal.

REFERENCES

- [1] S. Nussinov and W. Wetzel, Phys. Rev. D **36**, 130 (1987); M. B. Voloshin and M. A. Shifman, Sov. J. Nucl. Phys. **45**, 292 (1987) and **47**, 511 (1988); N. Isgur and M. B. Wise, Phys. Lett. **B232**, 113 (1989) and **237**, 527 (1990); H. Georgi, Phys. Lett. **B240**, 447 (1990). See M. Neubert, Phys. Rep. **245**, 259 (1994) for an extensive list of references.
- [2] G. T. Bodwin, E. Braaten and G. P. Lepage, Phys. Rev. D **51**, 1125 (1995).
- [3] G. P. Lepage *et al.*, Phys. Rev. D **46**, 4052 (1992).
- [4] B. A. Thacker and G. P. Lepage, Phys. Rev. D **43**, 196 (1991).
- [5] C. T. H. Davies, hep-lat/9705039.
- [6] S. Catterall *et al.*, Phys. Lett. **B300**, 393 (1993) and Phys. Lett. **B321**, 246 (1994).
- [7] C. T. H. Davies *et al.*, Phys. Rev. D **50**, 6963 (1994).
- [8] T. Manke *et al.*, hep-lat/9706003.
- [9] C. T. H. Davies *et al.*, Phys. Lett. **B345**, 42 (1995).
- [10] C. T. H. Davies *et al.*, hep-lat/9703010; to appear in Phys. Rev. D .
- [11] NRQCD collaboration, in preparation.
- [12] H. D. Trottier, Phys. Rev. D **55**, 6844 (1997).
- [13] G. P. Lepage, hep-lat/9707026 and references therein.
- [14] G. Parisi, in High Energy Physics 1980, XX Int Conf., Madison (1980), ed. L. Durand and L. G. Pondrom, AIP, New York (1981).
- [15] G. P. Lepage and P. B. Mackenzie, Phys. Rev. D **48**, 2250 (1993).
- [16] M. Lüscher *et al.*, Nucl. Phys. **B491**, 323 (1997).
- [17] G. S. Bali, K. Schilling and A. Wachter, Phys. Rev. D **56**, 2566 (1997); A. Wachter, PhD. thesis, Wuppertal report WUB_DIS 96-21 (1996).
- [18] A. Barchielli, E. Montaldi and G. M. Prosperi, Nucl. Phys. **B296**, 625 (1988); A. Barchielli, N. Brambilla and G. M. Prosperi, Nuovo Cimento **103A**, **N.1**, 59 (1990); Y.-Q. Chen, Y.-P. Kuang and R. J. Oakes, Phys. Rev. D **52**, 264 (1995).
- [19] N. Eicker, U. Glässner, S. Güsken, H. Hoerber, Th. Lippert, G. Ritzenhöfer, K. Schilling, G. Siegert, A. Spitz and A. Wachter (SESAM collaboration), ‘First Evidence of N_F -Dependence in the QCD Interquark-Potential’, Phys. Lett. **B383**, 98 (1996).
- [20] SESAM collaboration, ‘SESAM and T χ L Results for Wilson Action – A Status Report’, hep-lat/9707004; and ‘Critical Dynamics of the Hybrid Monte Carlo’, in preparation.
- [21] N. Eicker, U. Glässner, S. Güsken, H. Hoerber, P. Lacock, Th. Lippert, G. Ritzenhöfer, K. Schilling, G. Siegert, A. Spitz, P. Ueberholz, J. Viehoff (SESAM collaboration), ‘Light Quark Masses with Dynamical Fermions’, Phys. Lett. B (in print), hep-lat/9704019.
- [22] H. Hoerber (for the SESAM collaboration), ‘Light Quark Physics with Dynamical Fermions’, talk given at Lattice ’97, Edinburgh; to be published in Nucl. Phys. Proc. Suppl.; and N. Eicker, U. Glässner, S. Güsken, H. Hoerber, P. Lacock, Th. Lippert, G. Ritzenhöfer, K. Schilling, G. Siegert, A. Spitz, P. Ueberholz,

- J. Viehoff (SESAM collaboration), ‘Hadron Spectrum in Full QCD with two Flavours of Dynamical Wilson Fermions’, in preparation.
- [23] C. T. H. Davies *et al.*, Phys. Rev. Lett. **73**, 2654 (1994).
 - [24] W. H. Press *et al.*, “Numerical Recipes in C” (2nd edition), Cambridge University Press (1992).
 - [25] B. Grinstein and I. Z. Rothstein, Phys. Lett. **B385**, 265 (1995).
 - [26] J. Shigemitsu, Nucl. Phys. Proc. Suppl. **53**, 16 (1997); hep-lat/9608058.
 - [27] R. M. Barnett *et al.*, Phys. Rev. D **54** (Particle Data Booklet), 1 (1996).
 - [28] T. Manke *et al.*, talk given at Lattice ’97, Edinburgh; to be published in Nucl. Phys. Proc. Suppl.; hep-lat/9709001.
 - [29] G. P. Lepage and H. D. Trottier, talk given at Lattice ’97, Edinburgh; to be published in Nucl. Phys. Proc. Suppl.
 - [30] C. Morningstar, Phys. Rev. D **50**, 5902 (1994).

FIGURES

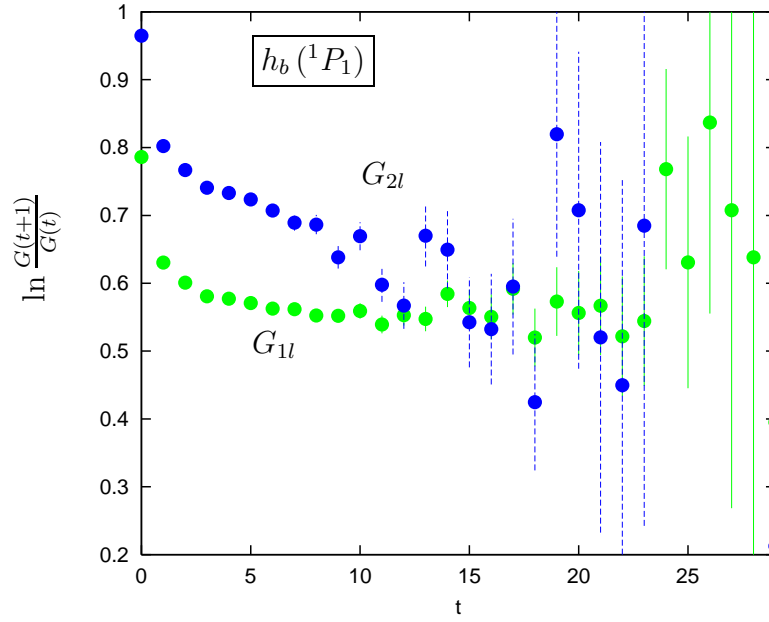
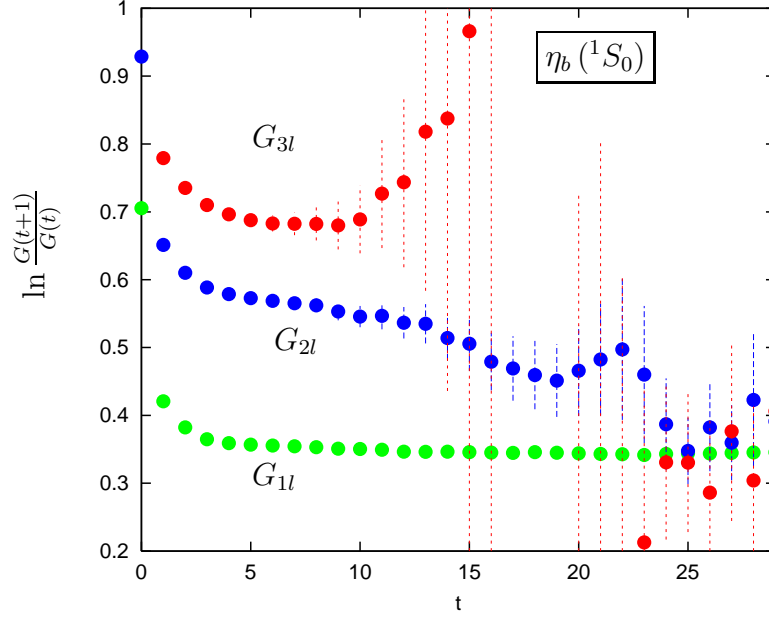


FIG. 1. Two examples of effective masses with several radial excitations. The η_b is at our lightest sea-quark, $\kappa = 0.1575$ whereas the h_b is at the heaviest, $\kappa = 0.156$.

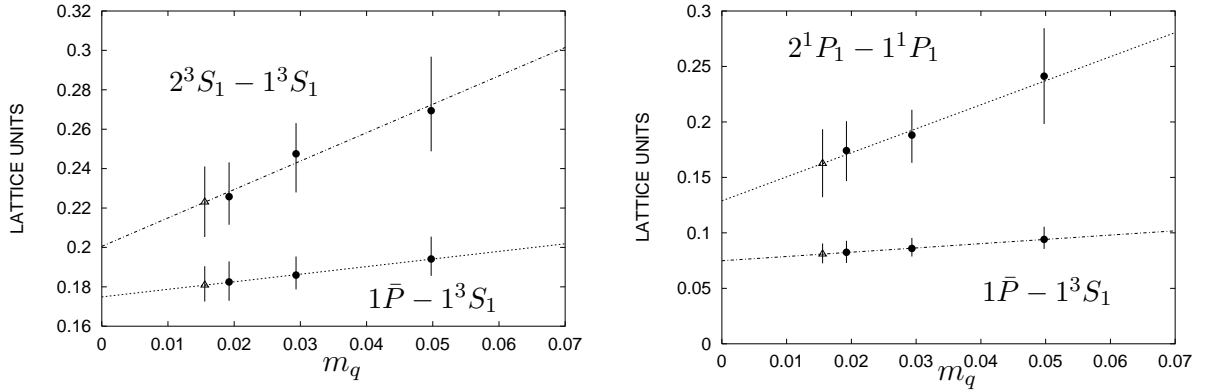


FIG. 2. Extrapolation of spin independent splittings to $m_s/3$. The $1\bar{P} - 1^3S_1$ splitting is plotted for comparison as it is one of the splittings used to determine the scale (it is shifted downward by 0.1 on the right plot). The triangular symbol denotes the extrapolated value.

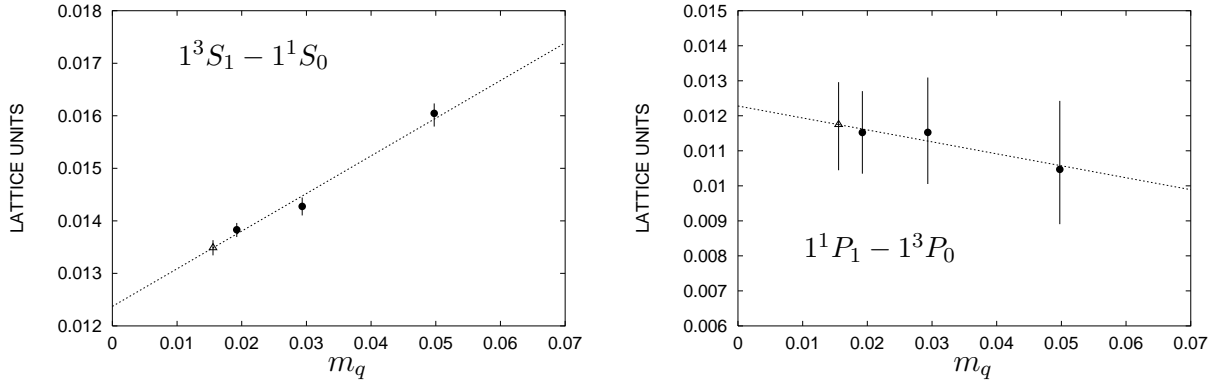


FIG. 3. Extrapolation of spin splittings to $m_s/3$. The triangular symbol denotes the extrapolated value.

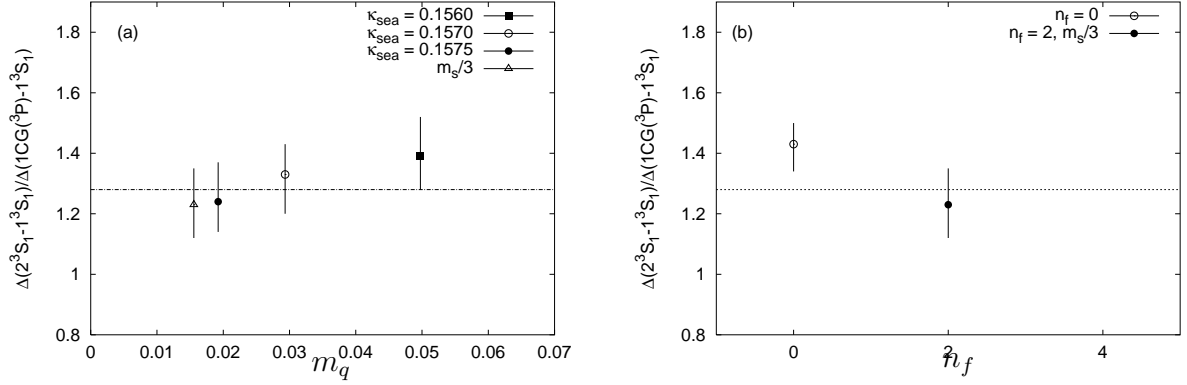


FIG. 4. The ratio of splittings $2^3S_1 - 1^3S_1$ to $1\bar{P} - 1^3S_1$ as a function of dynamical quark mass and number of dynamical quark flavours.

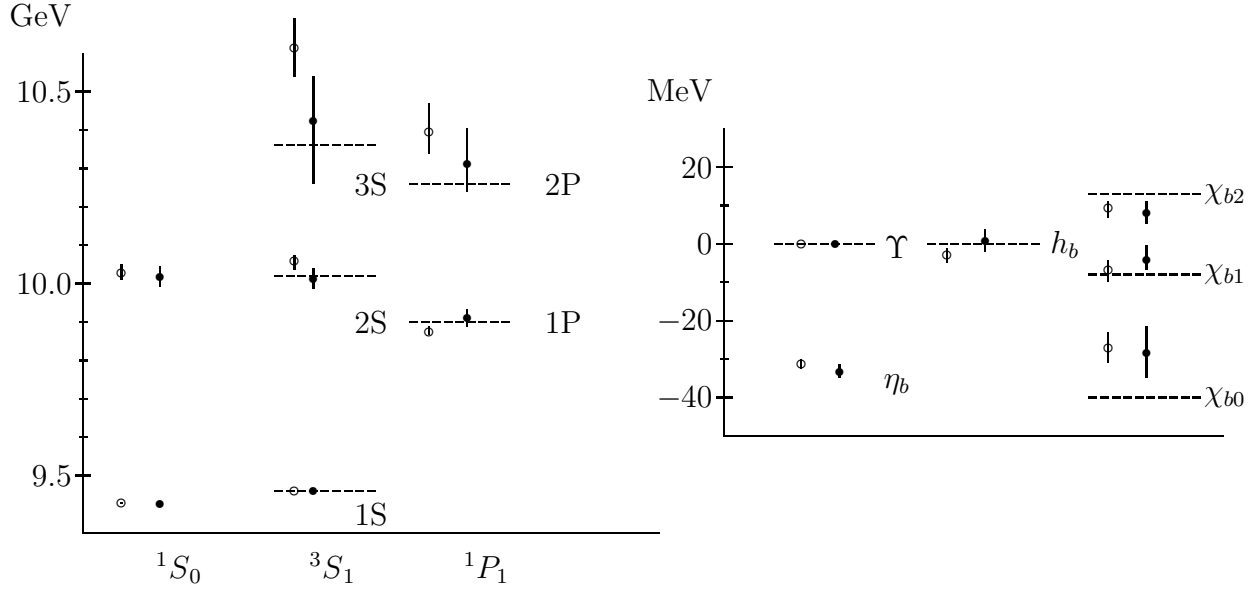


FIG. 5. The $b\bar{b}$ spectrum. The left plot shows radial splittings as well as angular momentum splittings with the Υ -level set to its physical value. The right plot resolves the fine structure: here the zero of energy is set to the Υ -level in the left part and to the spin averaged triplet P -level in the right part. Data points are labeled as follows: open circles : $n_f = 0, \beta = 6.0$; filled circles : $n_f = 2, m_q = m_s/3$.

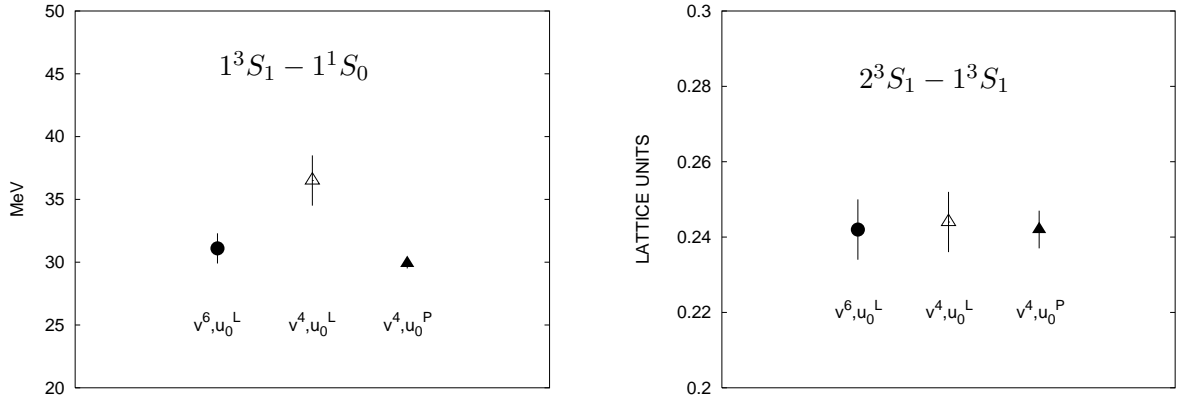


FIG. 6. On the left we compare the hyperfine S-splitting obtained with an $\mathcal{O}(M_b v^6)$ to the one obtained with an $\mathcal{O}(M_b v^4)$ correct NRQCD action. The higher order result is shifted significantly downward. Also shown (point on the very right) is the result obtained with an $\mathcal{O}(M_b v^4)$ action but using the plaquette tadpole scheme. The effect is to push the result down relative to the one obtained with the Landau gauge mean link tadpole scheme. On the right the same comparisons are shown for the spin-independent $2S - 1S$ splitting: as expected, no change is seen. All results are for the quenched case with $\beta = 6.0$.

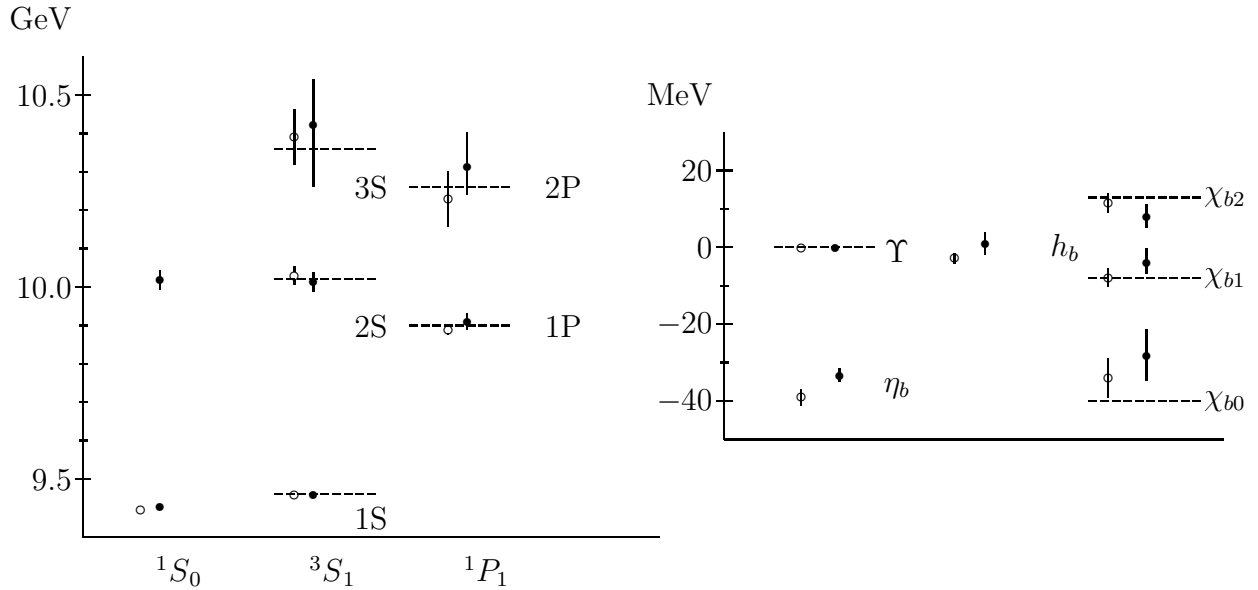


FIG. 7. Comparison of our $\{\mathcal{O}(mv^6), u_0^{(L)}\}$ Wilson-fermion result extrapolated to $m_s/3$ (full circles) to the $\{\mathcal{O}(mv^4), u_0^{(P)}\}$ (open circles) staggered fermion result at $m_q = 0.01$ of the NRQCD collaboration.

TABLES

TABLE I. Comparison of tadpole improvement schemes.

u_0	$\kappa = 0.156$	$\kappa = 0.157$	$\kappa = 0.1575$	quenched
$u_0^{(P)} = \sqrt[4]{\langle \frac{1}{3} \text{Tr} U_{\mu\nu} \rangle}$	0.8688	0.8695	0.8697	0.8778
$u_0^{(L)} = \langle \frac{1}{3} \text{Tr} U_\mu \rangle$	0.8499	0.8519	0.8529	0.8608

TABLE II. Operators and naming scheme.

$\bar{b}\bar{b}$	$2^{S+1}L_J(J^{PC})$	Ω
η_b	$^1S_0(0^{-+})$	1
Υ	$^3S_1(1^{--})$	σ_i
h_b	$^1P_1(1^{--})$	Δ_i
χ_{b0}	$^3P_0(0^{++})$	$\sum_{j=1}^3 \Delta_j \sigma_j$
χ_{b1}	$^3P_1(1^{++})$	$\Delta_i \sigma_j - \Delta_j \sigma_i$
χ_{b2}	$^3P_2(2^{++})$	$\Delta_i \sigma_i - \Delta_j \sigma_j$
		$\Delta_i \sigma_j + \Delta_j \sigma_i$
$\bar{\chi}$	$CG(^3P) \equiv \bar{P} = \frac{5^3 P_2 + 3^3 P_1 + 3^3 P_0}{9}$	-

TABLE III. Simulation details (n_f denotes the number of flavours).

	$\beta_{\text{dyn}} = 5.6, n_f = 2, 16^3 \times 32$		
κ_{sea}	0.156	0.1570	0.1575
number of configurations	200	200	200
measurements	800	800	800
	$\beta_{\text{quenched}} = 6.0, n_f = 0, 16^3 \times 32$		
	number of configurations: 200		
	measurements: 800		

TABLE IV. Spectrum results in lattice units for all three sea-quark masses and for the quenched simulation.

Level	$n_f = 2, \beta = 5.6$			$n_f = 0, \beta = 6.0$
	$\kappa = 0.1560$	$\kappa = 0.1570$	$\kappa = 0.1575$	
1^1S_0	0.3493(8)	0.3476(7)	0.3446(7)	0.3309(8)
2^1S_0	0.635(20)	0.613(15)	0.588(18)	0.574(12)
1^3S_1	0.3651(9)	0.3621(9)	0.3582(9)	0.3438(8)
2^3S_1	0.635(21)	0.610(15)	0.584(17)	0.586(13)
3^3S_1			0.75(5)	0.81(2)
1^1P_1	0.559(11)	0.548(9)	0.541(10)	0.512(9)
2^1P_1	0.80(4)	0.74(2)	0.71(2)	0.72(2)

TABLE V. Splittings at fixed sea-quark as well as quenched results (in lattice units).

Splitting	$n_f = 2, \beta = 5.6$			$n_f = 0, \beta = 6.0$
	$\kappa = 0.1560$	$\kappa = 0.1570$	$\kappa = 0.1575$	
$2^1S_0 - 1^1S_0$	0.285(20)	0.266(9)	0.243(7)	0.243(8)
$2^3S_1 - 1^3S_1$	0.269(25)	0.248(15)	0.226(17)	0.242(13)
$3^3S_1 - 1^3S_1$			0.39(6)	0.47(2)
$1^1P_1 - 1^3S_1$	0.194(10)	0.186(9)	0.183(10)	0.168(9)
$2^1P_1 - 1^1P_1$	0.24(4)	0.19(2)	0.17(2)	0.21(2)
$1\bar{P} - 1^3S_1$	0.194(11)	0.186(9)	0.182(10)	0.169(9)
$1^3S_1 - 1^1S_0$	0.0160(2)	0.0143(2)	0.0138(2)	0.0126(2)
$1^3P_2 - 1^1P_1$	0.0046(10)	0.0031(10)	0.0032(10)	0.0050(6)
$1^1P_1 - 1^3P_1$	0.0023(11)	0.0028(9)	0.0017(6)	0.0016(8)
$1^1P_1 - 1^3P_0$	0.0105(19)	0.0115(15)	0.0115(11)	0.0098(8)
$1^3P_2 - 1\bar{P}$	0.0039(8)	0.0036(7)	0.0033(5)	0.0038(5)
$1\bar{P} - 1^3P_1$	0.0029(9)	0.0023(7)	0.0017(6)	0.0027(7)
$1\bar{P} - 1^3P_0$	0.0111(15)	0.0110(13)	0.0115(11)	0.0110(9)
$1\bar{P} - 1^1P_1$	0.0006(7)	-0.0005(7)	-0.0001(5)	0.0011(4)

TABLE VI. Splitting results (in lattice units) extrapolated to $m_s/3$.

Splitting	$\Delta m(m_s/3)$	Δm_0
$2^1S_0 - 1^1S_0$	0.238(9)	0.212(18)
$2^3S_1 - 1^3S_1$	0.223(18)	0.201(29)
$1^1P_1 - 1^3S_1$	0.181(9)	0.176(16)
$2^1P_1 - 1^1P_1$	0.16(3)	0.13(5)
$1\bar{P} - 1^3S_1$	0.181(9)	0.175(16)
$1^3S_1 - 1^1S_0$	0.0135(2)	0.0124(3)
$1^3P_2 - 1^1P_1$	0.0029(9)	0.0021(15)
$1^1P_1 - 1^3P_1$	0.0019(7)	0.0015(13)
$1^1P_1 - 1^3P_0$	0.0117(13)	0.0123(22)
$1^3P_2 - 1\bar{P}$	0.0032(6)	0.0029(9)
$1\bar{P} - 1^3P_1$	0.0016(7)	0.0010(11)
$1\bar{P} - 1^3P_0$	0.0114(12)	0.0116(21)
$1\bar{P} - 1^1P_1$	-0.0003(5)	-0.0007(10)

TABLE VII. Determination of the lattice spacing from the $2^3S_1 - 1^3S_1$ and $CG(^3P) - 1^3S_1$ splittings. We use the average value to convert our results to physical units. R_{SP} is to be compared to the experimental value of 1.28.

	Splitting	$a^{-1}[\text{GeV}]$	Average $a^{-1}[\text{GeV}]$	R_{SP}
$n_f = 0, \beta = 6.0$	$\Upsilon' - \Upsilon$	2.33(10)	2.47(10)	1.43(9)
	$\bar{\chi} - \Upsilon$	2.61(13)		
$\kappa = 0.1560$	$\Upsilon' - \Upsilon$	2.09(18)	2.18(12)	1.39(13)
	$\bar{\chi} - \Upsilon$	2.27(12)		
$\kappa = 0.1570$	$\Upsilon' - \Upsilon$	2.27(15)	2.32(10)	1.33(12)
	$\bar{\chi} - \Upsilon$	2.36(10)		
$\kappa = 0.1575$	$\Upsilon' - \Upsilon$	2.49(17)	2.45(12)	1.24(13)
	$\bar{\chi} - \Upsilon$	2.41(10)		
$m_s/3$	$\Upsilon' - \Upsilon$	2.52(20)	2.48(14)	1.23(11)
	$\bar{\chi} - \Upsilon$	2.43(12)		

TABLE VIII. Overview of our results in physical units for full QCD and the quenched case.

Splitting	Simulation Result [GeV]		Experiment [27]
	$m_s/3$	$n_f = 0, \beta = 6.0$	
$2^1S_0 - 1^1S_0$	0.591(26)	0.600(20)	
$2^3S_1 - 1^3S_1$	0.553(25)	0.598(20)	0.5629
$3^3S_1 - 1^3S_1$		1.15(7)	0.895
$1^1P_1 - 1^3S_1$	0.450(22)	0.416(13)	
$2^1P_1 - 1^1P_1$	0.40(8)	0.52(7)	
$1\bar{P} - 1^3S_1$	0.448(22)	0.419(12)	0.4398
$1^3S_1 - 1^1S_0$	0.0334(19)	0.0313(12)	
$1^3P_2 - 1^1P_1$	0.0071(25)	0.0122(15)	
$1^1P_1 - 1^3P_1$	0.0046(18)	0.0039(20)	
$1^1P_1 - 1^3P_0$	0.0291(30)	0.0243(21)	
$1^3P_2 - 1\bar{P}$	0.0080(15)	0.0094(12)	0.0130
$1\bar{P} - 1^3P_1$	0.0040(18)	0.0067(15)	0.0083
$1\bar{P} - 1^3P_0$	0.0283(35)	0.0271(20)	0.040
$1\bar{P} - 1^1P_1$	-0.0009(15)	0.0028(10)	